Evaluation of local strain evolution from metallic whisker formation

Yong Sun,[a] Elizabeth N. Hoffman,[b,*] Poh-Sang Lam[b] and Xiaodong Li[a,*]

[a]Department of Mechanical Engineering, University of South Carolina, 300 Main Street, Columbia, SC 29202, USA
[b]Savannah River National Laboratory, Aiken, SC 29808, USA

The evolution of local strain on electrodeposited tin films upon aging has been monitored by digital image correlation (DIC) for the first time. Maps of principal strains adjacent to whisker locations were constructed by comparing pre- and post-growth scanning electron microscopy images. Results showed that the magnitude of the strain gradient plays an important role in whisker growth. DIC visualized the dynamic growth process in which the alteration of strain field has been identified as causing growth of subsequent whiskers.
© 2011 Published by Elsevier Ltd. on behalf of Acta Materialia Inc.

Electronic device failure caused by spontaneous whisker growth from solder and plating materials has been known for over a half century [1]. Such a phenomenon can be highly detrimental in microelectronic circuits, where devices are separated by spacings as small as tens of nanometers. Historically, lead has been added to solders to prevent whisker growth. Due to the harmful effects on human health and environments, it is no longer a valid solution to prevent whisker growth with lead. With the shift to whisker-prone "Pb-free" solders, controlling whisker growth from low-melting-point metals has again become technically challenging.

It is generally acknowledged that internal stresses arising in low-melting-point metals, such as Sn, In, Cd, Bi and Zn, promote whisker growth through a creep-like process [2]. Continuous effort has been made to search for a mechanism for whisker growth, and several theories [3–6] have been put forth. While uncertainty remains pertaining to the stress source or sources responsible for whisker growth, it is generally agreed that (i) whiskers grow from the root [7]; (ii) whisker growth is a result of a stress relaxation mechanism resulting from the underlying compressive stress [4,8]; and (iii) a thin film of low-melting-point metal promotes whisker growth [9]. The introduction of reliable lead-free solders into microelectronics manufacturing requires a deeper understanding of this failure mechanism, which is complicated by several potential driving forces in the multi-material system.

In order to fully comprehend the driving force(s) of whisker growth, several analytic methods, i.e. X-ray diffraction (XRD) [10] and synchrotron measurement [4,11], as well as numerical method, i.e. the finite element method [12], have been applied for measuring residual strain in thin metallic films with whisker growth. However, each technique has its limitations, especially for the analytic methods. XRD is not able to measure the localized strain state, while synchrotron measurement is too delicate for multi-time observations throughout the growth process. Such a situation raises the question: is there a better way to monitor the local, yet dynamic, evolution of strain during the growth of whiskers? In the current study, such evolvement prior to and following the whisker growth was measured and evaluated with the aid of digital image correlation (DIC), for the first time to our knowledge. DIC is a capable tool for mapping local displacement and strain fields through computation of full-field displacements, strains and strain rates on a sample surface [13,14]. DIC offers a convenient way to simultaneously achieve both full field visualization and dynamic evaluation of the strain state at the local level, which can give an insight into the mystery and uncertainty of whisker growth.

Sn and SnPb thin films on Cu substrates were fabricated by electrodeposition (details of the process are supplied in the Supporting Materials). All the samples have a spherical grain feature, which is typical for electrodeposition. Traditionally, DIC has been employed in

* Corresponding authors. E-mail addresses: elizabeth.hoffman@srnl.doe.gov; lixiao@cec.sc.edu

the field of micro- and macroscale deformation measurement with optical microscope images. Due to diffraction limitation of optical images, such analysis has a spatial resolution limit greater than 1 μm. Recently, DIC has been extended to the submicron range along with high-magnification surface measurement tools such as scanning electron microscopy (SEM) and atomic force microscopy (AFM) [15–17]. In the current study, the DIC technique was integrated with SEM to monitor the local in-plane strain evolution on the sample surface before and after whisker growth. The SEM offers digital data storage, the ability to post-process data with a range of desirable spatial resolutions, and excellent depth of field. These provide the necessary conditions for equipment integration with the currently available DIC platforms to measure small displacements down to the scale of microns on the grains around the growing whiskers, which have a representative diameter of 2–5 μm in the current study.

The distinct spherical characteristics of thin film morphology can be used in place of an artificially applied speckle pattern without further modification on the sample surface. This unique feature is especially advantageous for the current application with DIC, since the artificial patterns or gratings will obscure the observation of local whisker activities. A series of images on identical locations of the samples were taken by SEM (Quanta 200, FEI) using a constant voltage of 30 kV and a constant spot size of 5 μm in consecutive sessions, before and after whiskers were visually present. The resolution of the images was held constant at 1024 × 968 pixels. During intervals between the contiguous SEM sessions, which were from 2 to ∼20 days, the samples were kept in an ambient environment (∼23 °C and ∼30–60% relative humidity without controlling the ambient atmosphere). Arrays of Vickers indentation marks were made at different locations. These depressed sites served as an additional sources of compressive stress in addition to the residual stress from film deposition, and as markers to identify the areas of observation during the SEM sessions. For the Sn thin film deposited on copper, hillocks/whiskers were visually identified a few days after deposition. In contrast, no observable whisker growth was found on SnPb thin films after a considerable period of time.

The images of the areas of interest were analyzed using Vic-2D DIC software (Correlated Solutions, Inc., Columbia, SC) for an incremental correlation. The images taken in the first session were used as reference images (initial state). All other images taken at later times from the same sample were compared to the reference image for constructing the two-dimensional surface in-plane displacement field, from which the strain distribution on the film surface could be calculated. It is widely accepted that whisker growth is a diffusion phenomenon driven by residual compressive stress [8]. In the case of a thin film, the localized stress state can be easily related to the strain field on the surface, which makes DIC an effective tool for visualizing the progression of surface stress generation and relaxation by measuring strain before and after whisker growth. Since a Sn finish on copper had the highest whisker growth rate, the majority of the DIC analysis were carried out on

pure Sn thin films. Another reason we focused on the pure Sn thin films is that these samples had a relatively flat surface. Since only a two-dimensional strain state could be evaluated by the DIC software used, it was necessary to minimize the out-of-plane strains by observing flat areas where possible.

When a whisker forms on the sample surface, its elongation causes large in- and out-of-plane displacements, which can serve as sources of displacement discontinuity similar to cracks in fracture. One of the technical challenges for monitoring the strain evolution is to overcome the error due to poor correlation from DIC near and at the root of a whisker. This issue can be avoided in some cases when the initial or early stage of the whisker growth is captured by SEM observation before the whisker significantly alters the local morphology. Figure 1 shows an area that was observed by SEM shortly after the deposition was complete, and 1, 15 and 20 days after deposition, respectively. It is observed that a whisker started growing after about 15–20 days (denoted by a circle and indicated by an arrow in Fig. 1d). The length of the whisker is relatively short in comparison to the other whiskers found outside of this area of interest (AOI), leading to a nearly unobstructed view of the adjacent morphology, which is a necessary condition for a valid DIC evaluation. The strain field around the whisker location was calculated from the displacement field. Instead of giving the strain components with respect to each image orientation ($\varepsilon_{xx}/\varepsilon_{yy}/\varepsilon_{xy}$), the principal strains ($\varepsilon_1/\varepsilon_2$) are presented since the elongation and compression of local grains are of the most interest in the case of whisker growth. The AOI was a rectangular region of ∼55 × 45 μm (162 × 132 pixels), with a subset size (L) of 35 × 35 pixels and a step size (δ) of 3 pixels. All the parameters were deliberately chosen for optimizing the image correlation coefficient.

Images taken 1 day after deposition were compared to the as-deposited ones and showed excellent correlation quality, with $\varepsilon_1/\varepsilon_2$ well below ±0.1%. Such results demonstrate the accuracy of the methodology and validate further correlation processes. The strain detected during the period of observation falls into a range of ±0.6%, indicating that the Sn grains near the whisker growth locations yield plasticity. Such a result is consistent with reported stress measurements [5,12]. From Figure 1c, moderate compressive strain was usually detected a couple of grains apart from the growth location, which is denoted by the open black circle in Figure 1d. Figure 1c clearly indicates that considerable compressive strain and strain gradient are present around the root of the spontaneously growing Sn whisker during the incubation period (see the open red circles in the figure). Note that there is a weak tensile strain near the specific location. This is consistent with the observations that the stress gradient [18] or residual strain gradient [11] can be responsible for the whisker growth instead of a sole compressive field. The current results imply that the strain or stress gradient would be a driving force for whisker growth, assuming that these gradients provide a path for rapid diffusion. The evolution of the strain during the initial growth of the whiskers is also intriguing. The strain contours in Figure 1d show a significant change from those in Figure 1c. It should
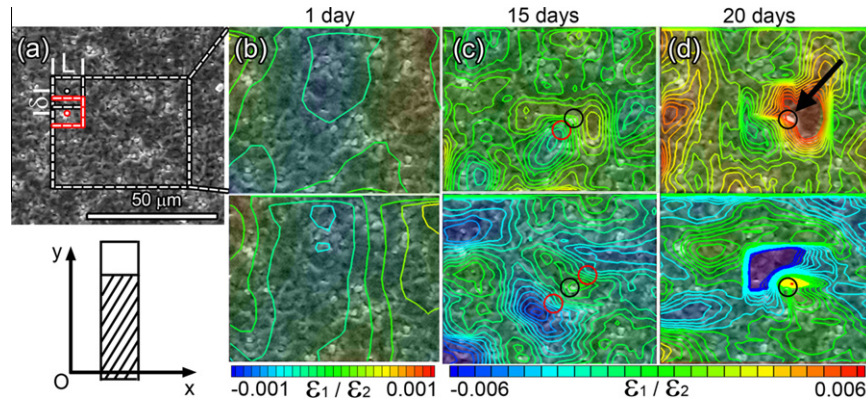
Figure 1. The reference image taken on a Sn film immediately after electrodeposition (a), with the AOI and subset outlined by a dotted line and the DIC results of ε_1 (first row) and ε_2 (second row) based on images taken at identical locations 1 day (b), 15 days (c) and 20 days (d) after deposition. The black circles/arrow in (c) and (d) denote the location of the whisker growth. The global coordinate system indicates the axial and transverse directions.
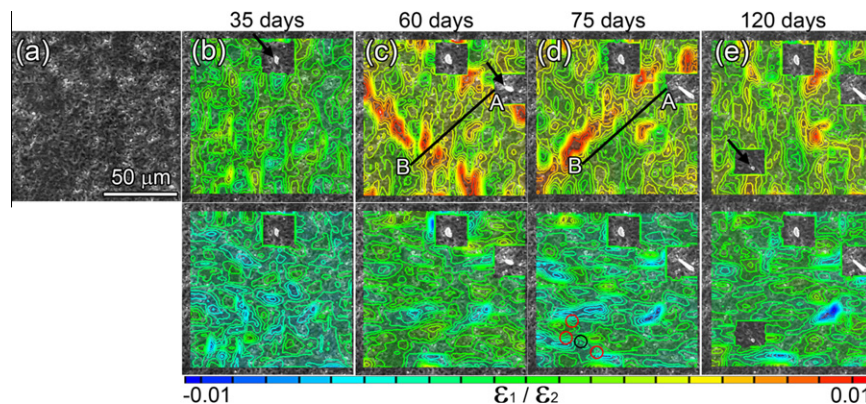

Figure 2. Another reference image taken on the Sn film immediately after electrodeposition (a), and DIC results of $\varepsilon_1/\varepsilon_2$ based on images taken at identical locations after 35 days (b), 60 days (c), 75 days (d) and 120 days (e).

be noted that the noticeable tensile strain on the location of whisker growth for ε_1 can be over-evaluated due to the displacement aroused by the elongation of the whisker. Nevertheless, distinct compressive strains were also present in a few locations, especially for ε_2.

A number of theories have been suggested as possible mechanisms for tin whisker growth, e.g. grain boundary diffusion [12,19], grain boundary fluid theory [8] and interface fluid flow [20], each of which has been supported by experimental observations in different cases. The considerable compressive found strain here can be caused by shrinkage of the grains, indicating that grain-boundary-related activity is the main factor in the growth process. The strain gradient around the whisker shown in Figure 1d (20 days) is much higher than that in Figure 1c (15 days), without any sign of relaxation of local strain due to whisker growth. This intensified strain gradient may serve as a sustainable driving force for whisker growth. This hypothesis is supported by the observation that a second whisker sprouted next to the existing whisker in about 40 days. However, the excessive morphology change did not allow a valid DIC measurement and therefore the strain distribution is not presented in this paper. (See the Supporting Materials for the appearance of the second whisker and the unsuccessful DIC calculation results.)

Conveniently, with mild modification, DIC can also capture the shift in the local strain state during the consecutive growth of whiskers. Furthermore, it provides a simple route to explore the inter-relationship between adjacent whiskers and thus to evaluate and visualize the uncertainties in consecutive growth processes. Figure 2 illustrates the sequence of consecutive growth of three whiskers observed at a different AOI on the same Sn film as in Figure 1. To analyze the strain state after whisker growth, rectangular areas covering the whiskers were cropped from the SEM images (Fig. 2b–e). This measure was necessary because the current DIC methodology is unable to correlate images with obstructed objects (in this case, the elongated whiskers) accurately, as mentioned earlier (see the Supporting Materials for DIC without cropping). The size of the cropped area was determined by the size of the subset used for the analysis with Vic-2D. In the present case, an AOI of 100×100 μm ($\sim 300 \times 300$ pixels) was selected, with a subset size of 39×39 pixels and a step size of 2 pixels. Multiple whiskers have been observed to grow successively out of the Sn surface during a period of 120 days. Images were taken after 35, 60, 75 and 120 days, respectively. Only mild principal strains were present around the first whisker. A generally compressive strain field can be seen in both principal directions
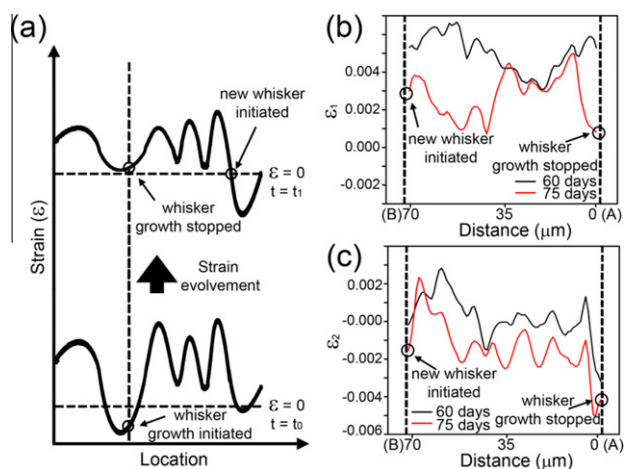
Figure 3. Sketch of the dynamic evolution of local strain leading to consecutive whisker growth (a) and actual line profiles of ε_1 (b) and ε_2 (c) extracted from the strain contour (A–B in Figs. 3c and 2d). The dotted lines in (b) and (c) indicate the locations of the whiskers.

around the second whisker prior to its growth. Figure 2c and d shows a wavy band-like trend of tensile strain for ε_1. This trend is postulated to be a sign of rapid diffusion of Sn atoms between adjacent locations caused by the growing whiskers. At the same time, a noticeable increase in compressive strain, especially ε_2, can be seen near the root of the third whisker, which is denoted by circles in Figure 2d. This trend eventually triggers the growth of the third whisker.

The growth process is depicted graphically in Figure 3a, where the first whisker grows at a location that is under considerable compressive strain and has a large strain gradient. As the whisker continues to grow, the Sn atoms from adjacent areas diffuse continuously to the root of the first whisker, resulting in the relaxation of local compressive strain and an increase in tensile strain and strain gradient. While the first whisker ceases to grow, the second whisker would be triggered if the strain gradient reaches a critical value. Such a dynamic pattern will lead to consecutive whisker growth in certain areas on the Sn film. Line profiles extracted from the DIC results appear to support this hypothesis, as shown in Figure 3b and c, where $\varepsilon_1/\varepsilon_1$ from location A to location B (Fig. 2b) is plotted. It is clear that the strain near location A is greatly relaxed to almost a neutral level, resulting in a decrease in whisker growth rate at this location. Meanwhile, a considerable strain gradient takes place near location B and is hypothetically responsible for the growth of the third whisker (see Fig. 2e) as a driving force for whisker growth. It should be noted that, although ε_1 near location B is still under tension after 75 days, the tension has been lowered to a level at which the compressive strain along the second principal direction (ε_2) dominates the whisker growth mechanism.

In summary, a methodology has been developed to incorporate a DIC technique with SEM images to map the local strain fields during whisker growth. By processing SEM images taken at consecutive time intervals over the AOI on Sn–Cu finishes, the local strain evolution due to whisker growth can be obtained. This methodology provides an alternative way to explore the complicated process of whisker growth through morphological changes. From the DIC results, it is proposed that the strain or stress gradient, instead of the overall compressive stress field, is the key for whisker growth. Results from SEM and DIC analysis also indicate that the whisker growth is a continuously dynamic process, during which growth of the subsequent whisker is triggered by the redistribution of the strain or stress field after local strain relaxation. The findings have advanced the understanding of whisker growth mechanisms and may provide insight for developing whisker mitigation technology for lead-free solder alloys.

[1] K.G. Compton, A. Mendizza, S.M. Arnold, Corrosion 7 (1951) 365–372.
[2] W.J. Boettinger, C.E. Johnson, L.A. Bendersky, K.W. Moon, M.E. Williams, G.R. Stafford, Acta Materialia 53 (2005) 5033–5050.
[3] K.N. Tu, Acta Metallurgica 21 (1973) 347–354.
[4] W.J. Choi, T.Y. Lee, K.N. Tu, N. Tamura, R.S. Celestre, A.A. MacDowell, Y.Y. Bong, L. Nguyen, Acta Materialia 51 (2003) 6253–6261.
[5] B.Z. Lee, D.N. Lee, Acta Materialia 46 (1998) 3701–3714.
[6] M.W. Barsoum, E.N. Hoffman, R.D. Doherty, S. Gupta, A. Zavaliangos, Physical Review Letters 93 (2004) 206104.
[7] S.E. Koonce, S.N. Arnold, Journal of Applied Physics 24 (1952) 365–366.
[8] K.N. Tu, J.C.M. Li, Materials Science and Engineering: A 409 (2005) 131–139.
[9] J.A. Nychka, Y. Li, F.Q. Yang, R. Chen, Journal of Electronic Materials 37 (2008) 90–95.
[10] J.H. Zhao, P. Su, M. Ding, S. Chopiri, P.S. Ho, IEEE Transactions on Electronics Packaging Manufacturing 29 (2006) 265–273.
[11] M. Sobiech, M. Wohlschlogel, U. Welzel, E.J. Mittemeijer, W. Hugel, A. Seekamp, W. Liu, G.E. Ice, Applied Physics Letters 94 (2009) 221901.
[12] E. Buchovecky, N. Jadhav, A.F. Bower, E. Chason, Journal of Electronic Materials 38 (2009) 2676–2684.
[13] M.A. Sutton, C. Mingqi, W.H. Peters, Y.J. Chao, S.R. McNeill, Image and Vision Computing 4 (1986) 143–150.
[14] F. Hild, S. Roux, Strain 42 (2006) 69–80.
[15] I. Chasiotis, W.G. Knauss, Experimental Mechanics 42 (2002) 51–57.
[16] X.D. Li, W.J. Xu, M.A. Sutton, M. Mello, IEEE Transactions on Nanotechnology 6 (2007) 4–12.
[17] Z.H. Xu, M.A. Sutton, X.D. Li, Acta Materialia 56 (2008) 6304–6309.
[18] J. Liang, Z.H. Xu, X.D. Li, Journal of Materials Science: Materials in Electronics 18 (2007) 599–604.
[19] K.N. Tu, Physical Review B 49 (1994) 2030–2034.
[20] H.P. Howard, J. Cheng, P.T. Vianco, J.C.M. Li, Acta Materialia 59 (2011) 1957–1963.